Supporting information

"Conformational lock" *via* unusual intramolecular C-F···O=C and C-H···Cl-C parallel dipoles observed in *in situ* cryocrystallized liquids

*Dhananjay Dey[a], Subhrajyoti Bhandary[a], Abhishek Sirohiwal[a], Venkatesha R. Hathwar[b] and Deepak Chopra[a]**

[a]*Crystallography and Crystal Chemistry Laboratory, Department of Chemistry, Indian Institute of Science Education and Research Bhopal, Bhopal By-Pass Road, Bhauri, Bhopal-462066, Madya Pradesh, India*

[b]*Center for Materials Crystallography, Department of Chemistry and iNANO, Aarhus University, Langelandsgade 140, Aarhus C DK-8000, Denmark*

Experimental procedure

All the difluorinated benzoyl chlorides (99.9 % pure) were purchased from Sigma Aldrich Company and used without further purification. Differential scanning calorimetry (DSC) experiments for all the liquids have been performed to set up the condition for *in situ* cryocrystallization. DSC plots of the difluoro benzoyl chlorides (including BC) have been shown in **Figure S1-S6**. In cooling curve liquid **24DFBC** solidified at -10.0ºC (263K) and during heating it melts at 16.9ºC (289.9K). Lindemann glass capillary (2 cm long and 0.3 mm diameter) was filled up with the liquid sample. Both the sides of the capillary sealed with glue and then mounted vertically on the goniometer under the liquid nitrogen nozzle as shown in the **Figure S7**. Using Oxford Cryostream plus controller, the temperature was cooled down at slow rate (70K/h) from the room temperature (298K).

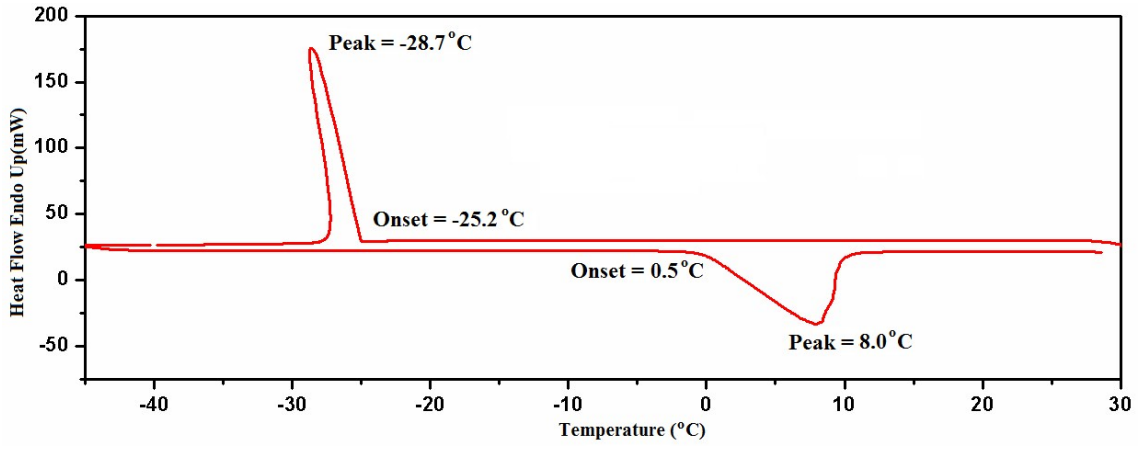

Figure S1. DSC plot of **BC** cooled/heated at 5ºC/min.

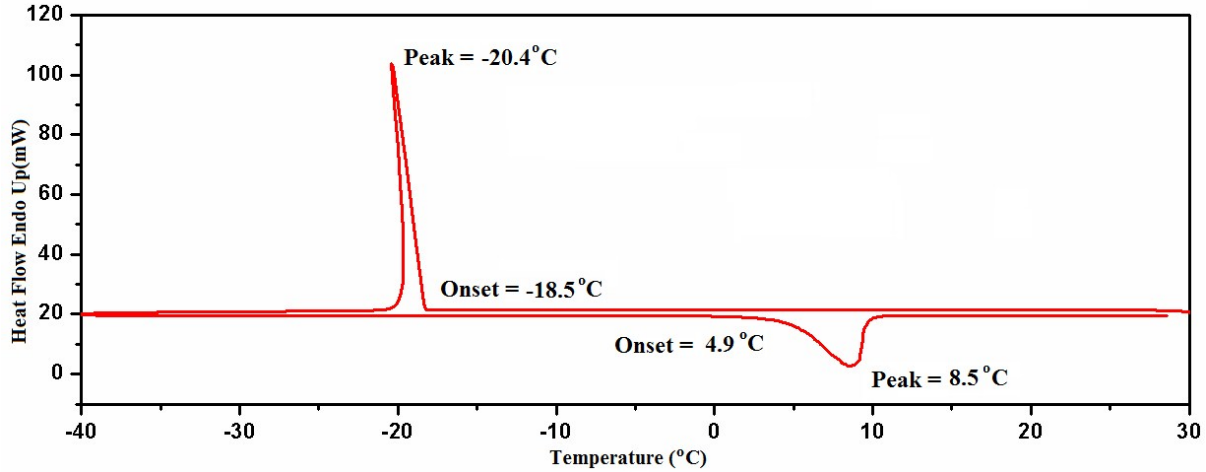

Figure S2. DSC plot of **2FBC** cooled/heated at 5ºC/min.

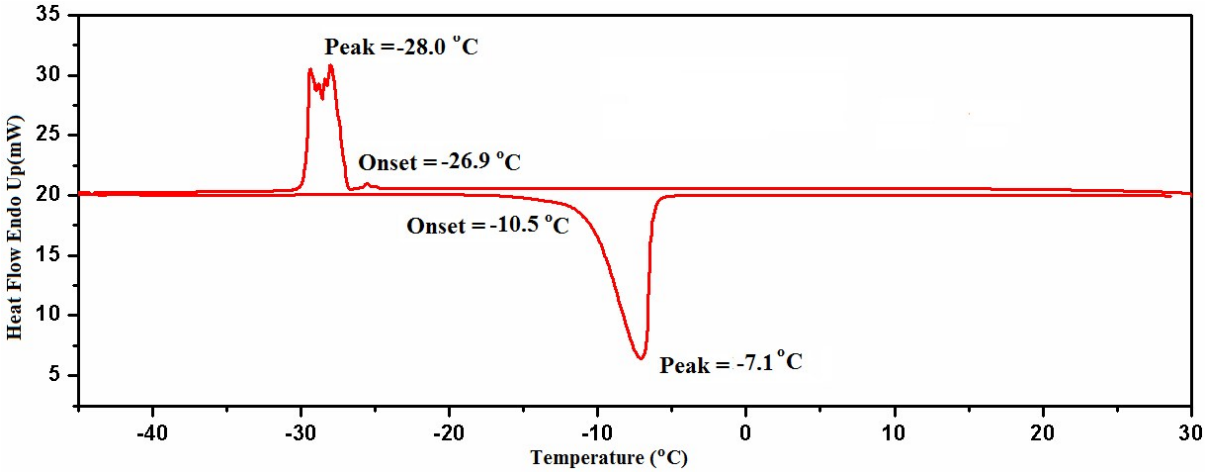

Figure S3. DSC plot of **23DFBC** cooled/heated at 5ºC/min.

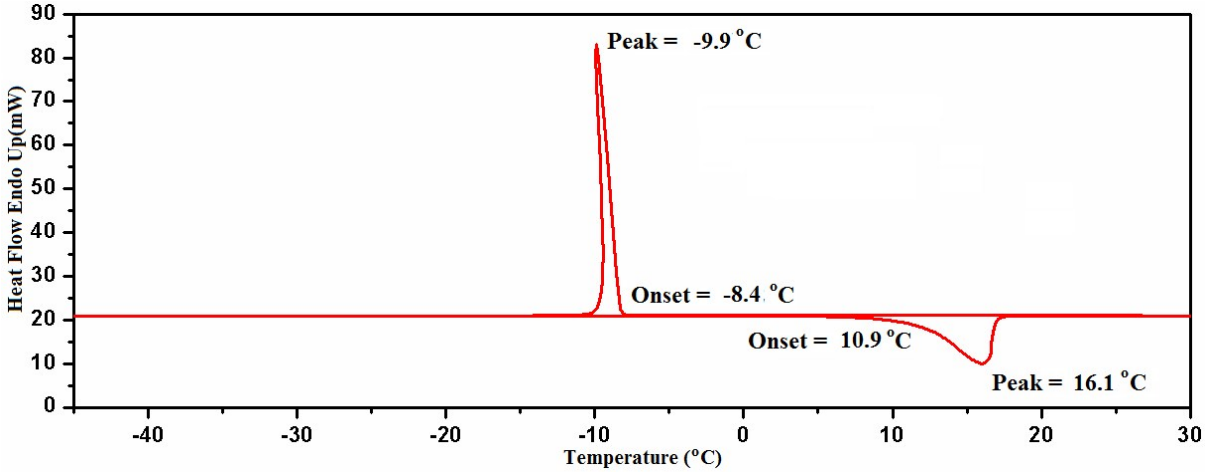

Figure S4. DSC plot of **24DFBC** cooled/heated at 5ºC/min.

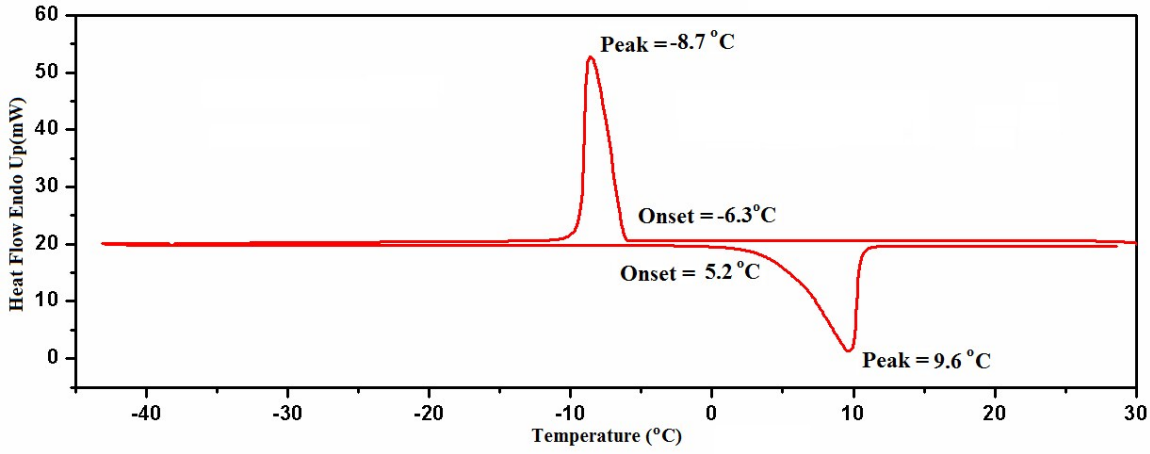

Figure S5. DSC plot of **25DFBC** cooled/heated at 5ºC/min.

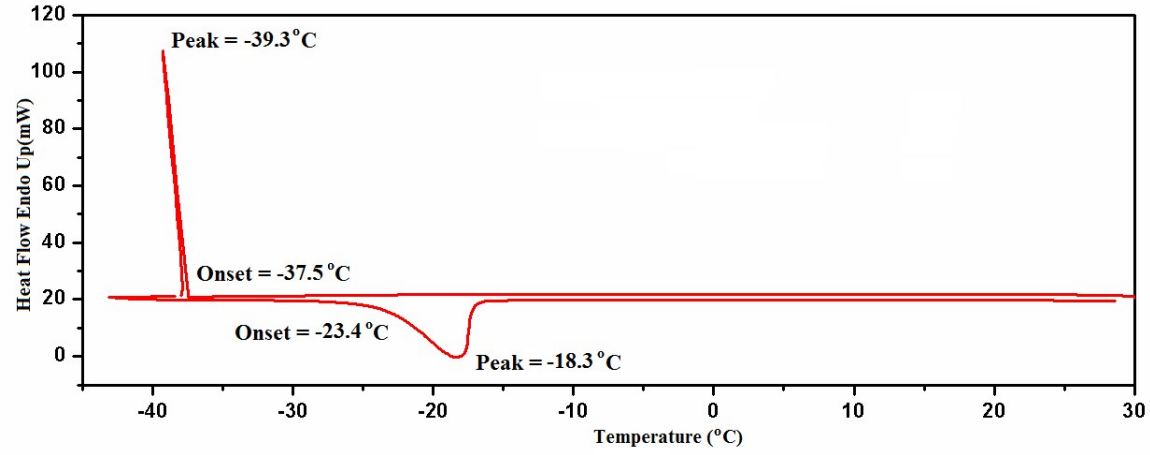

Figure S6. DSC plot of **26DFBC** cooled/heated at 5ºC/min.

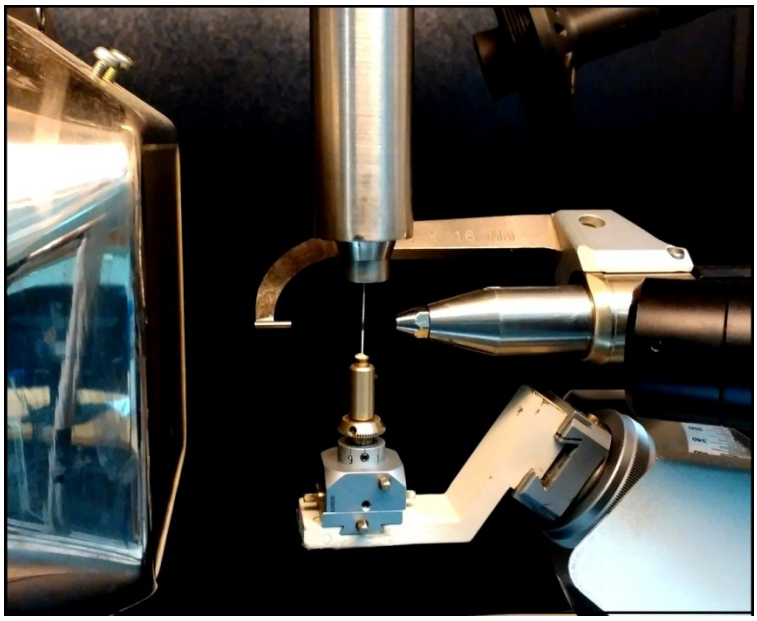

Figure S7. Instrumentation setup for the *in situ* cryocrystallization.

Table S1. Conditions (laser intensities and temperatures) for the crystallization of benzoyl chloride and fluoro substituted benzoyl chloride

Compound	Temperature	Ramp rate	Laser intensity		
			Output	Main	Fine
Benzoyl chloride *(Sigma Aldrich)*	245K	70K/h	41.6	14.9%	18.8%
2-Fluorobenzoyl chloride *(Sigma Aldrich)*	254K	100K/h	35.6	9.8%	22.4%
2,3-Difluorobenzoyl chloride *(Sigma Aldrich)*	245K	70K/h	36.0	11.0%	17.6%
2,4-Difluorobenzoyl chloride *(Sigma Aldrich)*	270K	70K/h	35.2	10.2%	18.8%
2,5-Difluorobenzoyl chloride *(Sigma Aldrich)*	265K	70K/h	27.6	7.8%	6.7%
2,6-Difluorobenzoyl chloride *(Sigma Aldrich)*	225K	70K/h	41.2	14.9%	23.9%

Figure S8. Optical Heating and Crystallization Device (OHCD).

In order to get quality crystals for single crystal X-ray diffraction, we have used Optical Heating and Crystallization device (OHCD) [1-2] (**Figure S8**). At 270K (-3ºC) the liquid (**24DFBC**) was converted into a polycrystalline solid slowly inside the capillary (**Figure S9**). Using OHCD, a molten zone was created inside the capillary with CO_2 laser to melt and reproduce the formation of the crystal. The laser power was increased slowly from zero to a particular value which was sufficient to melt the polycrystalline solid region at that temperature (270K). **Table S1** lists the conditions (temperatures, ramp rates and laser powers) for the growing crystal inside the capillary. Approximate 2 mm region of the capillary was selected for the crystallization. The melting region was slowly moved along the capillary length up and down (within 2 mm distance). The crystallization has been done moving the laser from the top to the bottom for all these fluorinated benzoyl chlorides. The

entire length of 2 mm of the capillary was scanned for 6h in all the cases to get good quality of the crystals. After the scan, we checked the crystal quality taking still images at 6 sec exposure time. **Figure S10** shows the crystal images inside the capillary and still images (diffraction pattern) of the respective liquid samples. The good quality of crystal was selected using X-ray diffraction. After that the crystal was cooled down to 110K at slow ramp rate (100K/h). To determine the unit cell parameters, 50 frames were collected with 6 sec exposure time using ω scan (ϕ = 0º). In some cases, single domain was not obtained inside the capillary. For that we have separated the individual domains using RLATT (reciprocal lattice). The reflections (in one type of domain) were indexed to get the crystal system and the unit cell parameters.

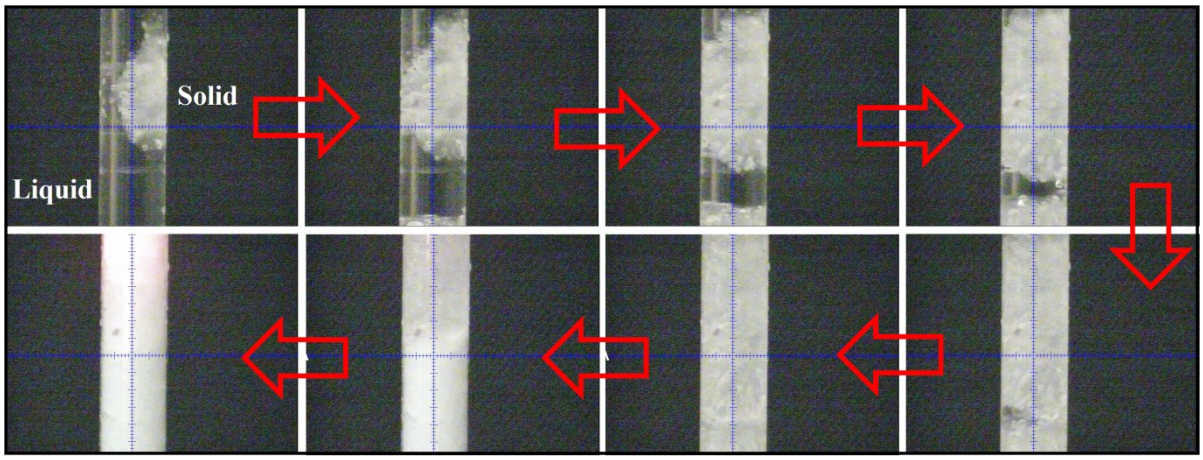

Figure S9. Solidification process of **24DFBC** at **270K** temperature under the liquid nitrogen flow (70K/h).

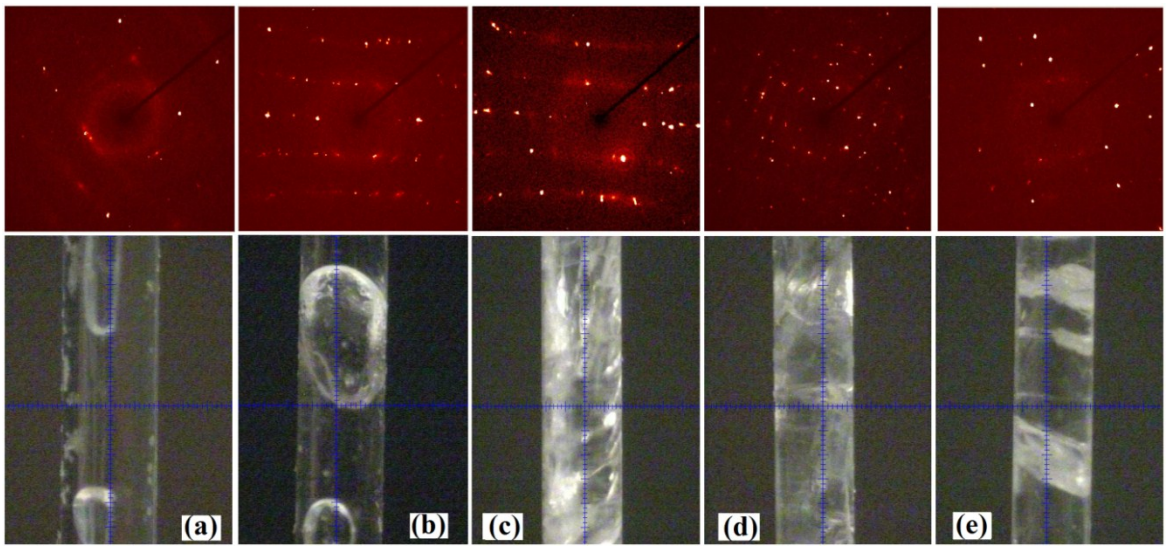

Figure S10. Still images and the corresponding crystals of (a) **BC** at 245K**,** (b) **2FBC** at 254K, (c) **24DFBC** at 110K**,** (d) **25DFBC** at 110K, (e) **26DFBC** at 110K temperature.

Data collection of structure refinements

All the single crystal diffraction data have been collected using a Bruker APEX II diffractometer equipped with a CCD detector using monochromated Mo Kα radiation (λ = 0.71073 Å) only with ω scan. The unit cell measurement, data collection, integration, scaling and absorption corrections for these forms were done using Bruker Apex II software [3]. The data collection was carried out giving an exposure time of 6 seconds per frame and at the crystal-to-detector distance is 60 mm. The intensity data were processed by using the Bruker SAINT [4] suite of programs. The crystal structures were solved by direct methods using SIR 2014 [5] and refined by the full matrix least squares method using SHELXL 2014 [6] present in the program suite WinGX (version 2014.1) [7]. Empirical absorption correction was applied using SADABS [8]. The non-hydrogen atoms were refined anisotropically and the hydrogen atoms bonded to C atom, were positioned geometrically and refined using a riding model with $U_{iso}(H) = 1.2U_{eq}$. The molecular connectivity was drawn using ORTEP32 [9] and the crystal packing diagrams were generated using Mercury 3.5.1 (CCDC) program [10]. Geometrical calculations were done using PARST [11] and PLATON [12]. The detailed crystallographic data and the structure refinement parameters were summarized in **Table S2**.

Table S2. Data collection of on the crystals and the structure refinement

Sample code	BC	2FBC	23DFBC	24DFBC	25DFBC	26DFBC
Formula	C_7H_5ClO	C_7H_4ClFO	$C_7H_3ClF_2O$	$C_7H_3ClF_2O$	$C_7H_3ClF_2O$	$C_7H_3ClF_2O$
Formula weight	140.56	158.55	176.54	176.54	176.54	176.54
Temperature/K	200(2)	110(2)	140(2)	110(2)	110(2)	110(2)
Wavelength (Å)	0.71073	0.71073	0.71073	0.71073	0.71073	0.71073
CCDC number	1440619	1440618	1452040	1426052	1426053	1426054
Crystal system	Monoclinic	Monoclinic	Triclinic	Monoclinic	Triclinic	Monoclinic
Space group	$P2_1/n$	$Pna2_1$	P-1	$P2_1/n$	P-1	$P2_1/c$
a (Å)	7.4705(5)	13.8205(6)	6.8590(9)	3.8289(2)	7.4814(4)	7.4388(2)
b (Å)	3.9581(2)	12.5452(6)	7.2006(9)	14.5220(6)	8.5648(4)	15.7661(3)
c (Å)	22.3439(12)	3.8197(2)	8.0365(9)	12.2527(5)	10.7372(6)	11.8282(2)
α (°)	90	90	94.613(9)	90	100.231(3)	90
β (°)	93.566(3)	90	104.275(9)	95.836(2)	95.404(3)	93.5970(10)
γ(°)	90	90	115.906(9)	90	91.365(3)	90
V(Å^3)	659.40(7)	662.26(6)	337.849(9)	677.76(5)	673.48(6)	1384.49(5)
Z'	1	1	1	1	2	2
Z	4	4	2	4	4	8
Density(g cm^{-3})	1.416	1.590	1.735	1.730	1.741	1.694

μ (mm^{-1})	0.482	0.510	0.530	0.529	0.532	0.518
F (000)	288	320	176	352	352	704
θ (min, max)	2.826, 28.695	2.192, 30.575	2.678, 28.273	2.181, 30.530	1.937, 27.877	2.155, 28.275
Treatement of hydrogens	Fixed	Fixed	Fixed	Fixed	Fixed	Fixed
$h_{min, max}$, $k_{min, max}$, $l_{min, max}$	(-5, 10), (-5, 4), (-26, 24)	(-19, 19), (-16, 17), (-3, 2)	(-9, 9), (9, -9), (10, -10)	(-2, 3), (-17, 20), (-17, 14)	(-7, 7), (-11, 11), (-14, 14)	(-7, 7), (-19, 21), (-15, 15)
No. of ref.	7678	3157	6690	8014	16476	44500
No. of unique ref./ obs. Ref.	1555, 1398	1324, 1236	1210, 1190	1435, 1328	2284, 2093	2661, 2554
No. parameters	82	91	100	100	199	199
R_all, R_obs	0.0559, 0.0514	0.0323, 0.0268	0.0258, 0.0254	0.0304, 0.0277	0.0375, 0.0345	0.0275, 0.0262
wR_2_all, wR_2_obs	0.1544, 0.1507	0.0673, 0.0601	0.0726, 0.0723	0.0763, 0.0734	0.092, 0.0964	0.0671, 0.0657
$\Delta\rho_{min, max}$ ($eÅ^{-3}$)	-0.235, 0.328	-0.272, 0.277	-0.270, 0.305	-0.236, 0.368	-0.260, 0.270	-0.275, 0.314
G. o. F.	1.112	1.096	1.158	1.089	1.099	1.035

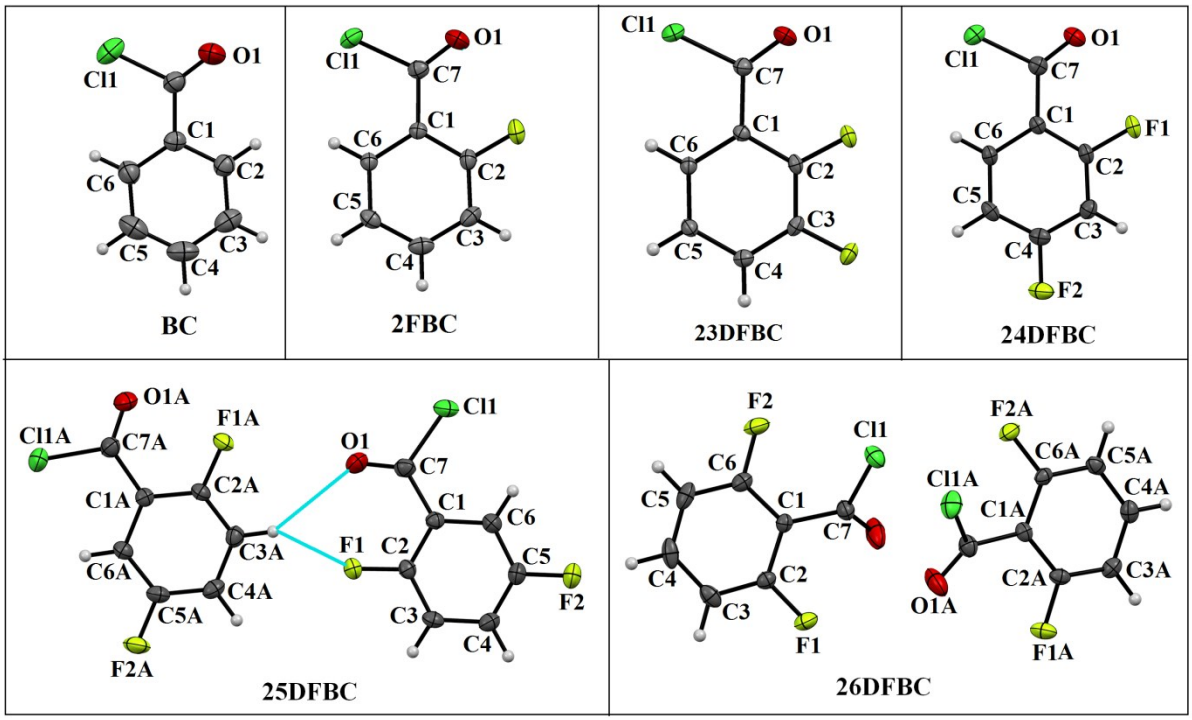

Figure S11. *ORTEP*s of benzoyl chloride and all the poly-fluoro substituted benzoyl chlorides drawn with 50% ellipsoidal probability.

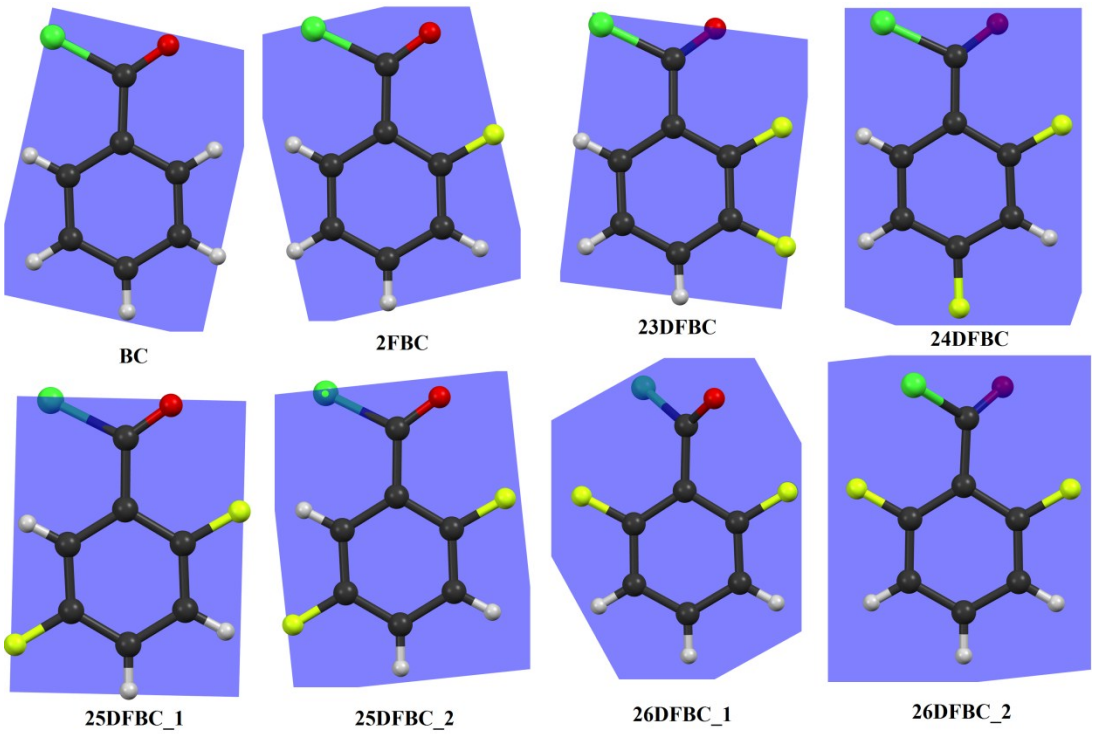

Figure S12. Molecular conformation shows the orientation of –COCl group in benzoyl chloride and the poly-fluoro substituted benzoyl chlorides with respect to the plane containing the phenyl ring.

All the molecular conformations were shown in a particular way such that the chlorine atom will be on the left side, and the oxygen atom will be on the right side. As the orientation of –COCl group with respect to the plane of the ring is not same for all the cases. So, there are total three possibilities: (i) deep red color for the oxygen atom (in the plane) and green color for the chlorine atom (in the plane); BC and 2FBC; (ii) clockwise rotation of -COCl group: deep red color for the oxygen atom (in front of the plane) and transparent blue color for the chlorine atom (back side of the plane); 25DFBC_1, 25DFBC_2 and 26DFBC_1; (iii) anti-clock rotation of -COCl group: deep violet color for the oxygen atom (back side of the plane) and green color for the chlorine atom (in front of the plane). 23DFBC, 24DFBC and 26DFBC_2.

Table S3. Molecular conformation: Dihedral angle (°) and Torsion angles (°) with respect to the phenyl ring.

Code	Dihedral angle	Torsion		
		Cl-C-C-C	Crystal	Optimized
BC	3.5	C2-C1-C7-Cl1	176.0(2)	180.0
2FBC	5.0	C2-C1-C7-Cl1	176.4(2)	-180.0
23DFBC	10.7	C2-C1-C7-Cl1	-169.3(1)	-179.8

24DFBC	12.4	C2-C1-C7-Cl1	-167.6(1)	180.0
25DFBC_1	17.0	C2-C1-C7-Cl1	163.0(2)	179.9
25DFBC_2	11.0	C2A-C1A-C7A-Cl1A	169.0(2)	-180.0
26DFBC_1	44.1	Cl1-C7-C1-C2	135.5(1)	127.4
26DFBC_2	42.7	Cl2A-C7A-C1A-C2A	-136.1(1)	-127.4

Cambridge Structural Database searches:

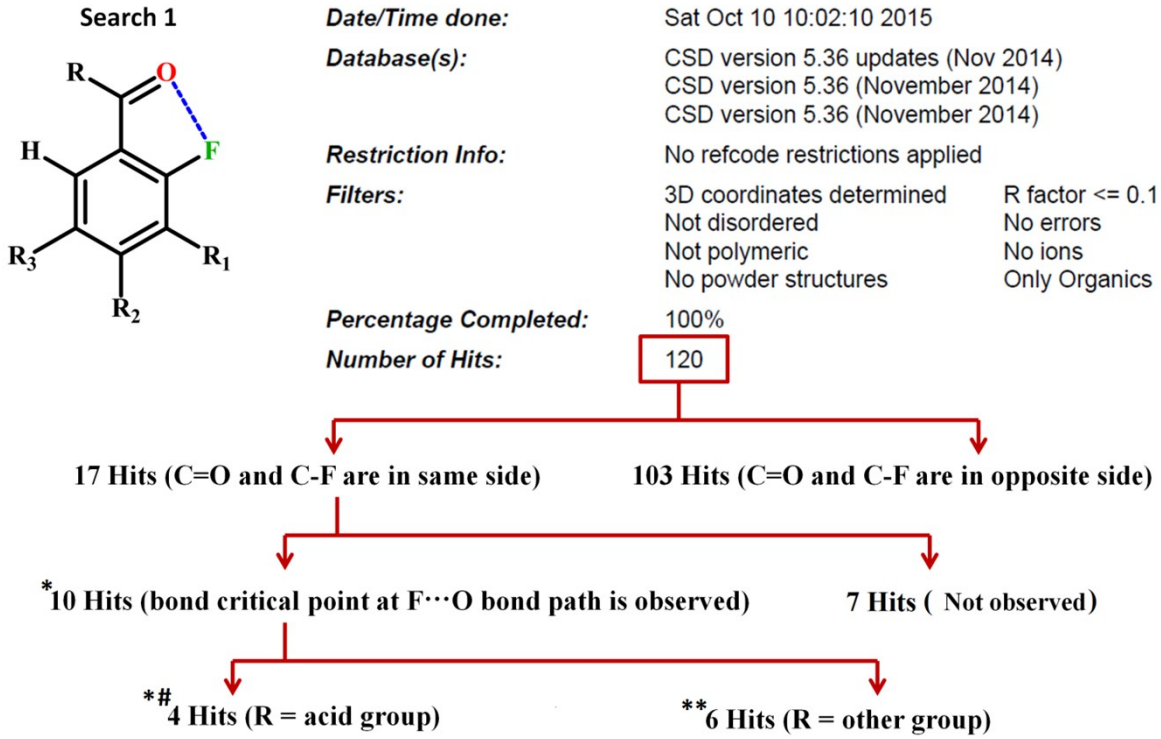

Table S4. List of molecules for intramolecular F···O contact with geometry obtained from CSD search

Serial no.	Refcode	Distance(Å)	Dihedral angle(°)
1	** BOMRIG [13]	2.740	29.8
2	** COTPUS [14]	2.703	11.8
3	** EVAJIV [15]	2.684	16.4
4	*# FBENZA02 [16]	2.682	10.7
5	** GAPJIS [17]	2.741	34.9
6	GEFWIZ [18]	2.740	40.5
7	*# GISZIS [19]	2.649	7.8
8	** HAWXEJ [20]	2.696	19.1
9	** HICFEE [21]	2.691	16.3
10	HUZCIO [22]	3.055	65.2
11	MUBKOK [23]	2.846	49.8
12	PAXYOE [24]	2.788	39.7
13	SAFQUN [25]	2.768	41.1
14	*# SUZNOR [26]	2.706	20.6
15	UPADUL [27]	2.792	39.1
16	UPAFUN [28]	2.889	49.5
17	*# XOJNAM [29]	2.696	4.4

QTAIM analysis

Furthermore, QTAIM [13-15] analysis for some selected dimers at the crystal geometry (with the hydrogen atoms moved to their neutral value) was performed at the MP2/6-311++G (d, p) level using Gaussian 09 [16]. The formatted checkpoint file (fchk) was used as input file for AIMALL (version 13.05.06) [17] calculation. The electron density features at the bond critical points, which are computed, is as follows: (i) electron density (ρ_b), (ii) Laplacian ($\nabla^2\rho_b$) and (iii) kinetic energy density (G_b). $DE^V(E_{int})$= -0.5 V_b (in au) [18]. Laplacian maps for various fluorosubstituted benzoyl chlorides are shown in **Figure S14**.

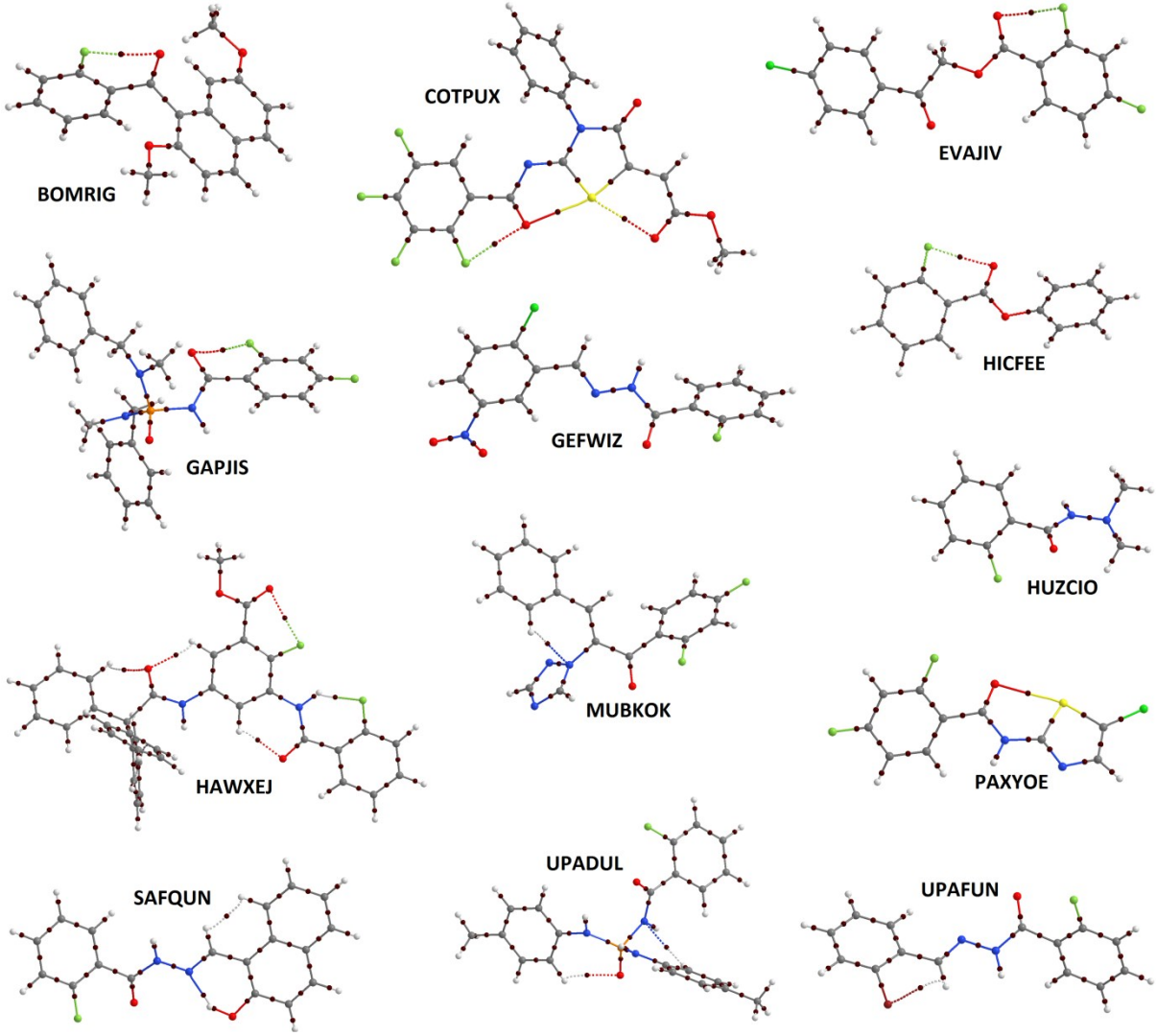

Figure S13. Molecular graphs for molecules (**) obtained from the CSD search depicting the intra-molecular F···O contact.

Table S5. Topological parameters at the BCP of Cl···H and Cl···F interaction

Code	R_{ij} (Å)	ρ_{BCP} (e/Å^3)	$\nabla^2\rho_{BCP}$ (e/Å^5)	V_b (au)	G_b (au)	DE^V (kcal/mol)
Cl···H						
BC	**2.79**	**0.094**	**1.378**	**-0.009565**	**0.011916**	**3.00**
BC (Opt)	***2.77***	***0.092***	***1.321***	***-0.009081***	***0.011380***	***2.85***
2FBC	**2.67**	**0.106**	**1.512**	**-0.010800**	**0.013230**	**3.39**
2FBC(Opt)	***2.67***	***0.103***	***1.430***	***-0.010120***	***0.012464***	***3.18***
2FBC* (XD)	**2.65**	**0.102**	**1.612**	**-0.010906**	**0.013801**	**3.42**
Cl···F						
26DFBC_1	**2.97**	**0.080**	**1.942**	**-0.009603**	**0.010983**	**3.01**
26DFBC_2	**2.92**	**0.089**	**1.325**	**-0.010807**	**0.012214**	**3.39**

Italicised values were obtained from optimized geometry.

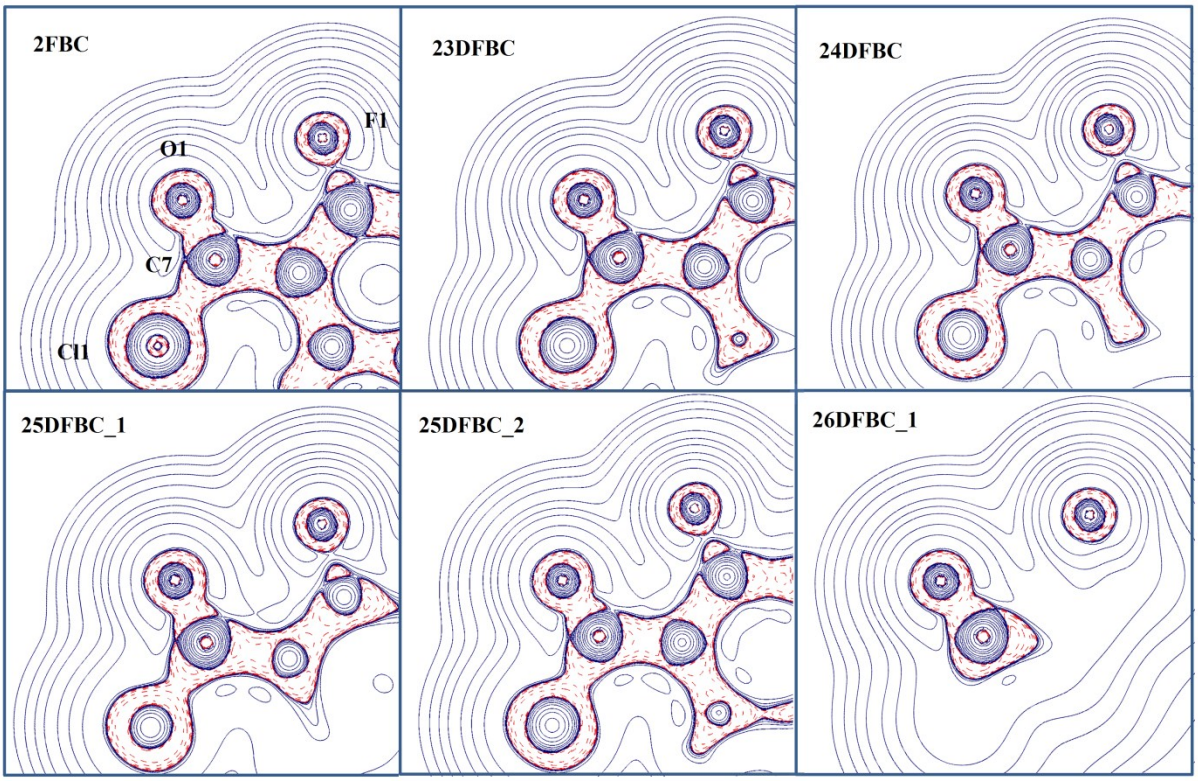

Figure S14. Laplacian map for all the poly-fluoro substituted benzoyl chlorides obtained from QTAIM analysis in the molecular plane defined by atoms O1, C7 and F1.

Theoretical calculation and Multipole refinement for 2FBC:

Single point periodic quantum mechanical calculations were carried out using CRYSTAL09 [36] at B3LYP/6−31G** level of theory [37] for the geometry obtained from the experimental structure determination as input. The shrinking factors (IS1-IS3) along with the reciprocal lattice vectors were set to 4 (27 k-points in irreducible Brillouin zone). The bi−electronic Coulomb and exchange series values for the truncation parameter were set as

ITOL1-ITOL4 = 7 and ITOL5 = 14, respectively. The level shifter was set to 0.7 Hartree/cycle for a better convergence. Upon convergence on energy (~10^{-6} Hartree), the periodic wave functions were obtained. Static theoretical structure factors were derived at the sin (θ/λ) = 1.1 $Å^{-1}$ resolutions using the XFAC module of CRYSTAL09. The atomic positions were held fixed to the values obtained from the experimental structure determination during the spherical atom model refinements. All theoretical structure factors were assigned to unit weights during the refinements based on the methodology followed in the literature [38]. The displacement parameters were set to zero to consider a static model and multipolar refinements of the theoretical data were carried out up to the octupole level. The charge density modeling and multipolar non−spherical atom refinements were performed with XD2006 [39] using the Hansen and Coppens multipole formalism [40]. The function minimized was $\Sigma w\{|F_o|^2 - K|F_c|^2\}^2$, for all reflections obtained theoretically. The core and valence scattering factors of all atoms were derived from Su, Coppens and Macchi wave functions [41]. The residual electron density maps (**Fig.S15**), plot of fractional dimension (d_f) vs residual density (ρ_0) (**Fig.S16**), molecular graph (**Fig.S17a**), electrostatic potential map (**Fig.S17b**) and NCI analysis (**Fig.S17c**) derived from the theoretical charge density modelling for **2FBC** are given below.

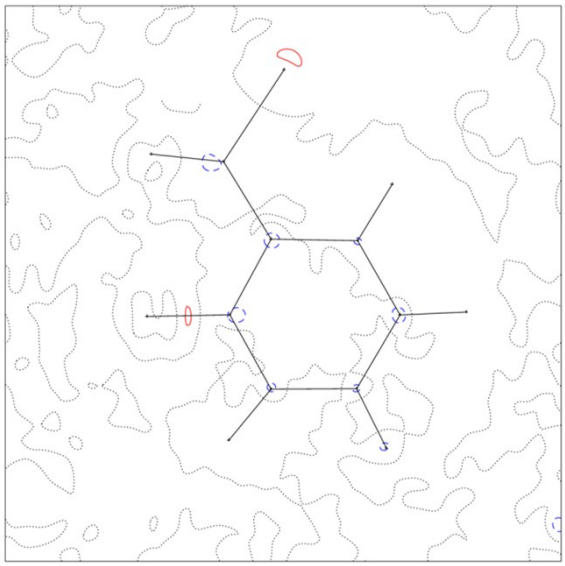

Figure S15. Residual electron density map obtained from the theoretical charge density models. Solid red lines indicate positive contours, dashed blue lines negative contours and dotted black lines depict zero contours. The contour intervals are at ±0.10 $eÅ^{-3}$.

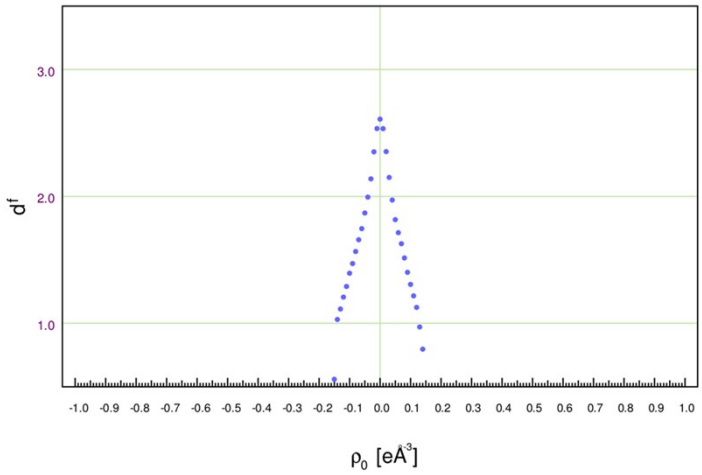

Figure S16. Plot of fractional dimension (d_f) vs residual density (ρ_0).

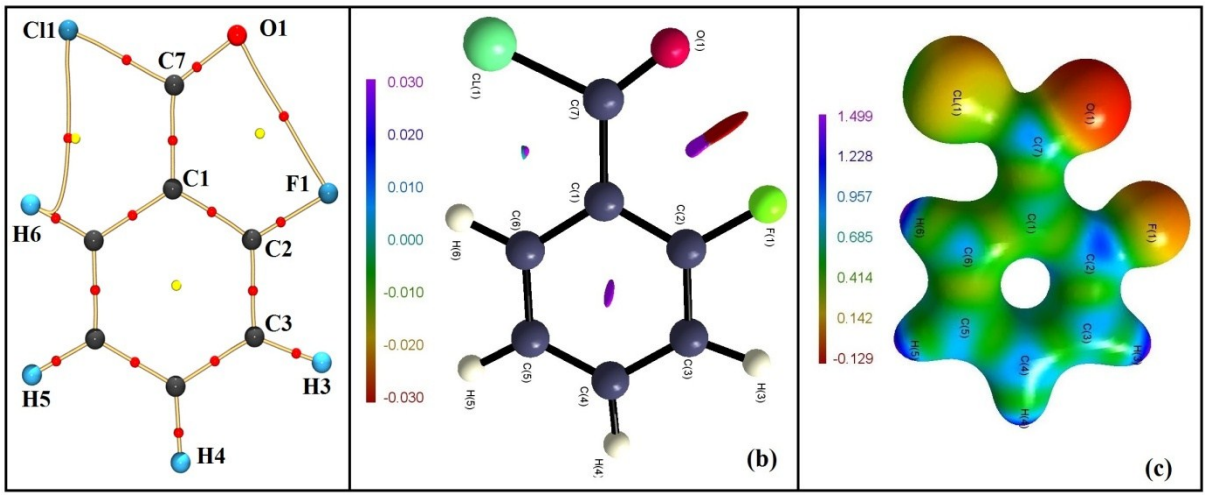

Figure S17. (a) Molecular graph obtained from theoretical multipole refinement for **2FBC**, (b) Electrostatic potential mapped in e/Å^{-3} unit from theoretical multipolar refinement, c) RDG isosurface for intramolecular F···O noncovalent interaction with s = 0.6 au. The color is plotted in the range of $-0.03 < \rho^{*}\text{sign}(\lambda_2) < 0.03$ au.

Distributed Atomic Polarizability Analysis

Distributed atomic polarizability has been calculated using QTAIM based topological partitioning of electron density for BC and 2FBC in isolated geometry extracted from crystal structure with C-H bond length fixed to 1.083Å using neutron diffraction values reported in literature [42]. For atomic polarizability calculation [43] at crystal geometry, wave functions were generated at MP2/6-311++G (d, p) level of theory in the presence electric field (0.005 au, directed at [±1, 0, 0], [0, ±1, 0], and [0, 0, ±1]) and absence of electric field (zero electric field). Weighting scheme was applied while calculating atomic polarizabilities in order to

avoid drastic change in the ellipsoid. Distributed atomic polarizabilities were calculated using *PolaBer* developed by Macchi and co-workers. Visualization was also performed with *PolaBer*.

Table S6: Calculated values of atomic charge, tensors components of atomic polarizability and volume of polarizability ellipsoid of oxygen, hydrogen and chlorine atoms present in BC and 2FBC. (Values are given in atomic units)

Code	Atom	q(oxygen)	α_{11}	α_{22}	α_{33}	α_{12}	α_{13}	α_{23}	α_{iso}	$V_a^{\#}$
BC	**O1**	**-1.097**	**7.901**	**3.668**	**7.389**	**-1.257**	**4.491**	**-1.347**	**6.319**	**128.768**
	H2	**0.065**	**1.679**	**0.837**	**3.274**	**-0.123**	**1.493**	**-0.234**	**1.930**	**45.635**
	Cl1	**-0.239**	**13.446**	**11.699**	**18.496**	**-2.466**	**-5.353**	**3.793**	**14.547**	**218.260**
	H6	**0.067**	**2.451**	**1.291**	**3.722**	**-0.824**	**-0.647**	**0.890**	**2.488**	**44.142**
2FBC	**O1***	**-1.057**	**5.795**	**9.905**	**4.770**	**2.418**	**1.719**	**2.525**	**6.824**	**125.224**
	Cl1	**-1.830**	**17.845**	**14.896**	**10.728**	**-6.110**	**2.412**	**-1.830**	**14.490**	**217.245**
	H6	**0.074**	**2.998**	**3.106**	**1.161**	**-0.940**	**0.955**	**-0.331**	**2.422**	**43.363**

* Oxygen atom involved in intramolecular F···O contact in compound **2FBC**. $^{\#}$Denote atomic volume bound by an electron density isosurface of 0.001 au.

NICS analysis

Nucleus-independent chemical shift (NICS) was calculated with the gauge-independent atomic orbital (GIAO) approach at the B3LYP/6-311+G(d,p) [44-45] level taking the optimized geometry. The NICS indices calculated at the center (ring critical point (3, +1) obtained from QTAIM analysis) of the five-member ring denoted as $NICS(0)_{zz}$ (out-of-plane component at Z-direction). Likewise, the NICS values at 1Å above the plane of the five-membered ring are denoted $NICS(1)_{zz}$. $NICS(1)_{zz}$ (out-of-plane component at Z-direction) is a measure of the π-electron delocalization, whereas NICS(0) is a combination of the σ + π-electron delocalization.

NCI analysis

NCImilano has been performed with name.wfn file using MP2/6-311G++(d, p) basis set in Gaussian 09. In input file, we have taken the grid size 0.03Å for the each step. It generated RDG and ρ*sign (λ_2) cube files with rho (ρ) cutoff value 0 to 0.02 au. Reduced density gradient (RDG) isosurface value was generated at 0.6 (s) and plotted in MoleCoolQt [46] software. The color scale of RDG surfaces is $-0.03 < \rho < 0.03$.

Table S7. Grid step size and rho (ρ) cutoff value to build RDG isosurface

Code	Isosurface (s)	Rho (ρ) cutoff (au)	Grid step (Å)	Points on X -axis	Points on Y-axis	Points on Z-axis
BC	**0.6**	**0 to 0.02**	**0.03**	**120**	**350**	**100**
2FBC	**0.6**	**0 to 0.02**	**0.03**	**120**	**350**	**100**
23FBC	**0.6**	**0 to 0.02**	**0.03**	**120**	**350**	**100**
24DFBC	**0.6**	**0 to 0.02**	**0.03**	**120**	**350**	**100**
25DFBC_1	**0.6**	**0 to 0.02**	**0.03**	**120**	**350**	**100**
25DFBC_2	**0.6**	**0 to 0.02**	**0.03**	**120**	**350**	**100**
26DFBC_1	**0.6**	**0 to 0.02**	**0.03**	**120**	**350**	**160**
26DFBC_2	**0.6**	**0 to 0.02**	**0.03**	**120**	**350**	**100**

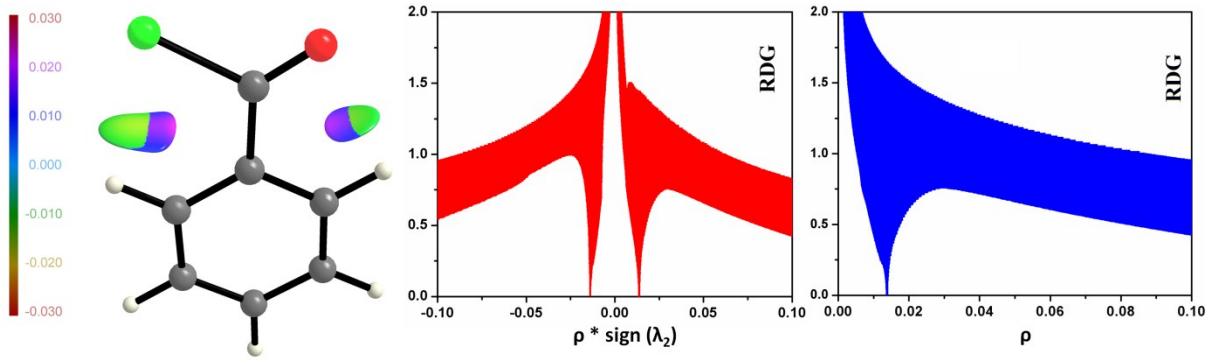

Figure S18. Plot of reduced density gradient (RDG) versus electron density multiplied by the sign of the second Hessian eigen value [ρ*sign (λ_2)] and electron density (ρ) for intramolecular Cl···H contact in **BC.**

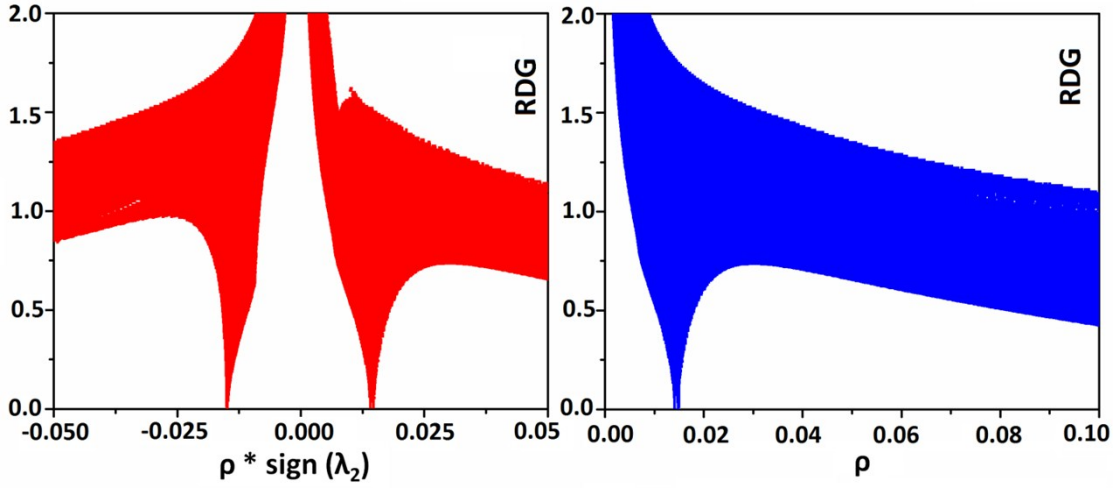

Figure S19. Plot of reduced density gradient (RDG) versus electron density multiplied by the sign of the second Hessian eigen value [ρ*sign (λ_2)] and electron density (ρ) for intramolecular F···O and Cl···H contact in **2FBC.**

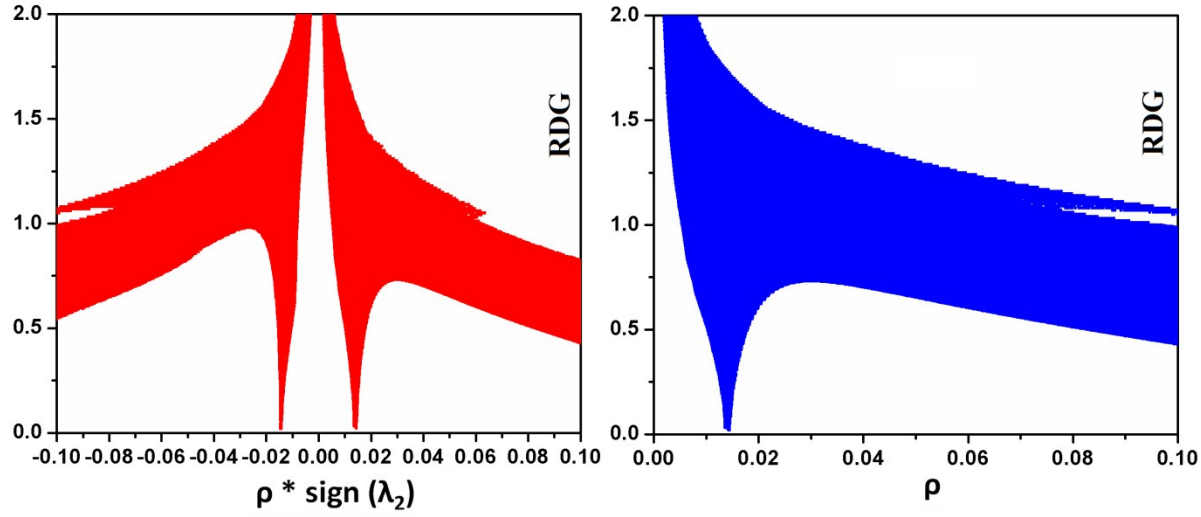

Figure S20. Plot of reduced density gradient (RDG) versus electron density multiplied by the sign of the second Hessian eigen value [ρ*sign (λ_2)] and electron density (ρ) for intramolecular F···O and Cl···H contact in **23DFBC**.

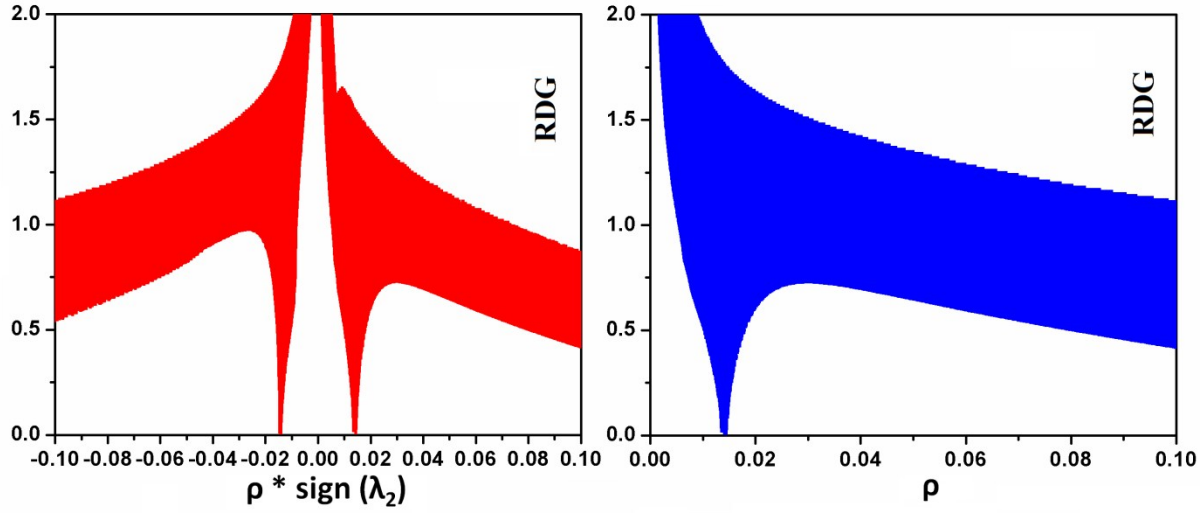

Figure S21. Plot of reduced density gradient (RDG) versus electron density multiplied by the sign of the second Hessian eigen value [ρ*sign (λ_2)] and electron density (ρ) for intramolecular F···O and Cl···H contact in **24DFBC**.

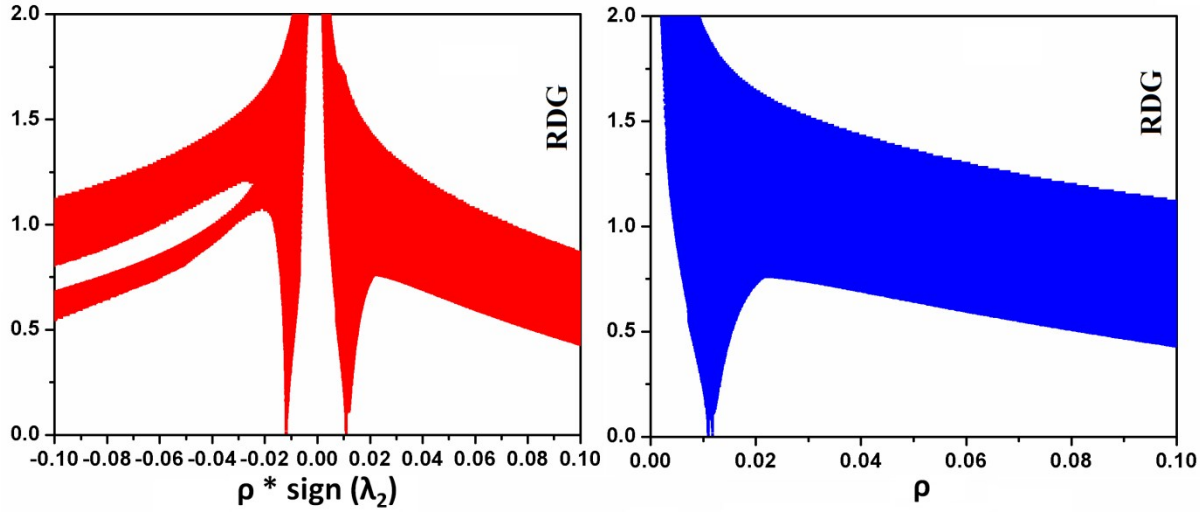

Figure S22. Plot of reduced density gradient (RDG) versus electron density multiplied by the sign of the second Hessian eigen value [ρ*sign (λ_2)] and electron density (ρ) for intramolecular F···O and Cl···H contact in **25DFBC_1**.

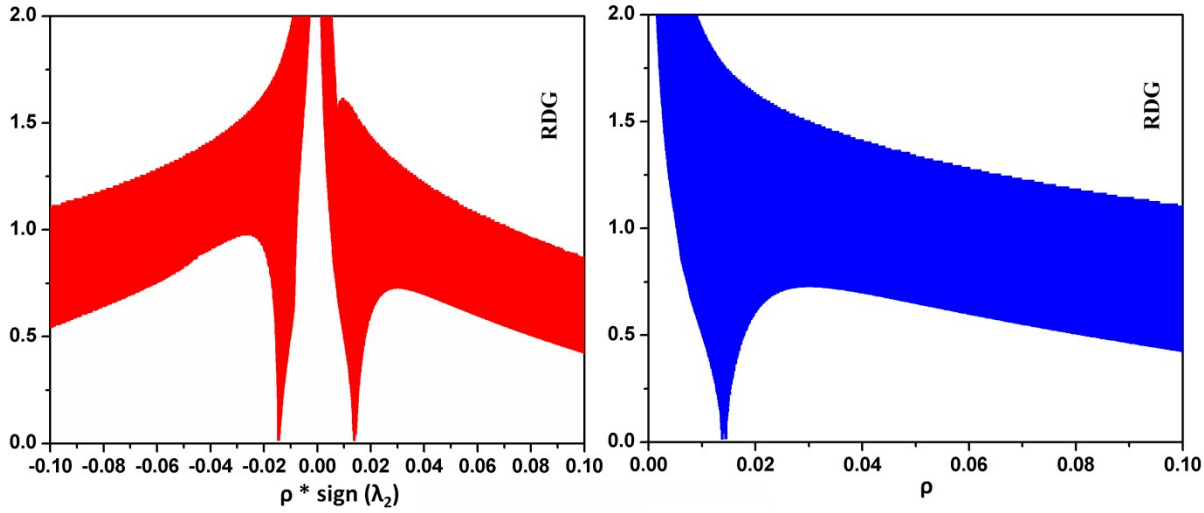

Figure S23. Plot of reduced density gradient (RDG) versus electron density multiplied by the sign of the second Hessian eigen value [ρ*sign (λ_2)] and electron density (ρ) for intramolecular F···O and Cl···H contact in **25DFBC_2**.

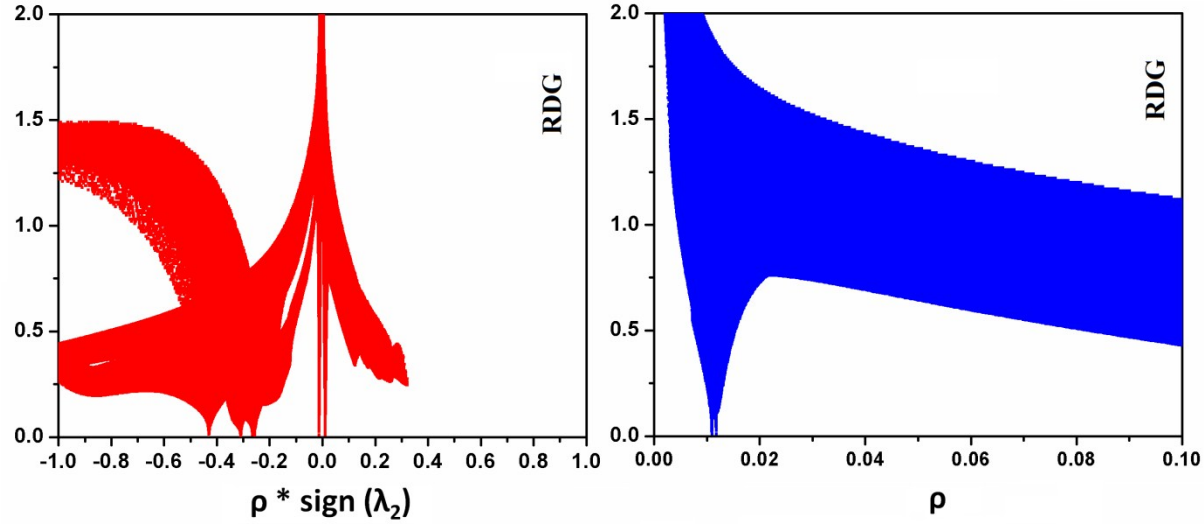

Figure S24. Plot of reduced density gradient (RDG) versus electron density multiplied by the sign of the second Hessian eigen value [ρ*sign (λ_2)] and electron density (ρ) for intramolecular F···O and Cl···F contact in **26DFBC_1**.

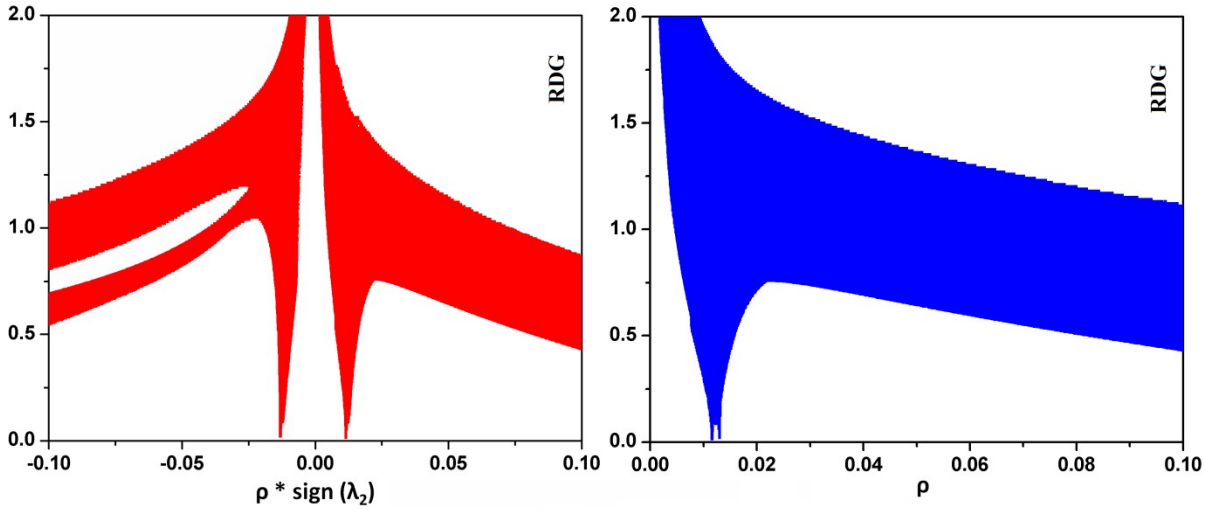

Figure S25. Plot of reduced density gradient (RDG) versus electron density multiplied by the sign of the second Hessian eigen value [ρ*sign (λ_2)] and electron density (ρ) for intramolecular F···O and Cl···F contact in **26DFBC_2**.

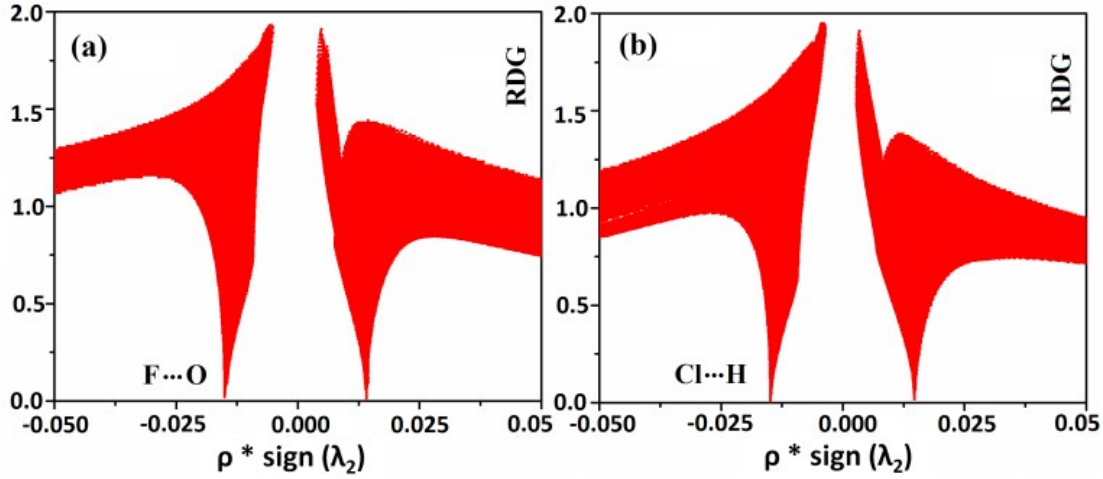

Figure S26. Plot of reduced density gradient (RDG) versus electron density multiplied by the sign of the second eigenvalue of Hessian matrix [ρ*sign (λ_2)] for intramolecular a) F···O and b) Cl···H contacts in **2FBC**.

References:

1. M. Nussbaumer, R. Boese, In *Correlations, Transformations, and Interactions in Organic Crystal Chemistry, IUCr Crystallography Sumposia, Vol 7*; Jones, W. D.; Katrusiak, A; Eds. Oxford, 1994, 20.

2. http://www.sci-ohcd.eu/

3. Apex2, Version 2 User Manual, M86-E01078, Bruker Analytical X-ray Systems Madison, WI, 2006.

4. Siemens, SMART System, Siemens Analytical X-ray Instruments Inc. Madison, MI, 1995.

5. M. C. Burla, R. Caliandro, B. Carrozzini, G. L. Cascarano, C. Cuocci, C. Giacovazzo, M. Mallamo, A. Mazzone and G. Polidori, *J. Appl. Crystallogr.* 2015, **48**, 306–309.

6. G. M. Sheldrick, *Acta Crystallogr.* 2008, **A64**, 112-122.

7. L. J. Farrugia, *J. Appl. Crystallogr.* 1999**, 32**, 837-838.

8. G. M. Sheldrick, SADABS; Bruker AXS, Inc.: Madison, WI, 2007.

9. L. J. Farrugia, *J. Appl. Crystallogr.* 1997, **30**, 565-566.

10. C. F. Macrae, I. J. Bruno, J. A. Chisholm, P. R. Edgington, P. McCabe, E. Pidcock, L. Rodriguez-Monge, R. Taylor, J. Streek, P. A. Wood, *J. Appl. Crystallogr.* 2008, **41**, 466-470.

11. M. Nardelli, *J. Appl. Crystallogr.* 1995, **28**, 659.

12. A. L. Spek, *Acta Crystallogr.* 2009, **D65**, 148-155.

13. S. Mohri, S. Ohisa, T. Tsumuki, N. Yonezawa, A. Okamoto, *Acta Crystallogr.* 2014, **E70**, 278.

14. G. N. Lipunova, E. V. Nosova, A. A. Laeva, T. V. Trashakhova, P. A. Slepukhin, V. N. Charushin, *Zh.Org.Khim.(Russ.)(Russ.J.Org.Chem.)* 2008, **44,** 749.

15. H. -K. Fun, S. Arshad, B. Garudachari, A. M. Isloor, M. N. Satyanarayan, *Acta Crystallogr.* 2011, **E67,** o1599.

16. V. R. Hathwar, T. S. Thakur, R. Dubey, M. A. Pavan, T. N. G. Row, G. R. Desiraju, *J. Phys. Chem. A,* 2011, **115***,* 12852-12863.

17. M. Pourayoubi, S. Shoghpour, L. Torre-Fernandez, S. Garcia-Granda, *Acta Crystallogr.* 2012, **E68,** o270.

18. E. Espinosa, E. Molins, C. Lecomte, *Chem. Phys. Lett.* 1998, **285**, 170−173.

19. A. A. Knapik, W. Minor, M. Chruszcz, *Acta Crystallogr.* 2008*,* **E64,** o466.

20. C. Li, S. -F. Ren, J. -L. Hou, H. –P. Yi, S. -Z. Zhu, X. -K. Jiang, Z. -T. Li, *Angew. Chem., Int. Ed.* 2005*,* **44**, 5725-5729.

21. M. Shibakami, A. Sekiya, *Acta Crystallogr.* 1995, **C51,** 326.

22. K. W. Muir, D. G. Morris, *Acta Crystallogr.* 2003, **E59,** o490

23. C. –Y. Yan, G. –Z. Wang, C. -H. Zhou, *Acta Crystallogr.* 2009*,* **E65,** o2054.

24. X. –W. Liu, J. –Y. Li, H. Zhang, Y. –J. Yang, J. –Y. Zhang, *Acta Crystallogr.* 2012, **E68,** o1857.

25. D. -Y. Wang, X. –F. Meng, J. –J. Ma, *Acta Crystallogr.* 2012*,* **E68,** o21.

26. C. E. Wagner, T. L. Groy, *Acta Crystallogr.* 2010, **E66,** o2340.

27. M. Pourayoubi, A. Tarahhomi, A. L. Rheingold, J. A. Golen, *Acta Crystallogr.* 2011, **E67**, o934.

28. D. –F. Zhang, D. -Y. Liu, C. –X. Li, S. –S. Huang, B. –J. Zhang, *Acta Crystallogr.* 2011*,* **E67,** o940.

29. T. S. Thakur, G. R. Desiraju, *Cryst.Growth Des.* 2008, **8,** 4031-4044.

30. R. F. W. Bader, *Atoms in Molecules: A Quantum Theory*, Oxford University Press, Oxford, U.K., 1990;

31. V. G. Tsirelson, *In The Quantum Theory of Atoms in Molecules: From Solid State to DNA and Drug Design*, ed. C. Matta and R. Boyd, Wiley-VCH, Weinheim, Germany, 2007, ch. 10. 45

32. E. Arunan, G. R. Desiraju, R. A. Klein, J. Sadlej, S. Scheiner, I. Alkorta, D. C. Clary, R. H. Crabtree, J. J. Dannenberg, P. Hobza, H. G. Kjaergaard, A. C. Legon, B. Mennucci, D. Nesbitt, *J. Pure Appl. Chem.* 2011, **83**, 1619-1636.

33. M. J. Frisch, G. W. Trucks, H. B. Schlegel, G. E. Scuseria, M. A. Robb, J. R. Cheeseman, G. Scalmani, V. Barone, B. Mennucci, G. A. Petersson, H. Nakatsuji, M. Caricato, X. Li, H. P. Hratchian, A. F. Izmaylov, J. Bloino, G. Zheng, J. L. Sonnenberg, M. Hada, M. Ehara, K. Toyota, R. Fukuda, J. M. HasegawaIshida, T. Nakajima, Y. Honda, O. Kitao, H. Nakai, T. Vreven, J. A. Jr. Montgomery, J. E. Peralta, F. Ogliaro, M. Bearpark, J. J. Heyd, E. Brothers, K. N. Kudin, V. N. Staroverov, R. Kobayashi, J. Normand, K. Raghavachari, A. Rendell, J. C. Burant, S. S. Iyengar, J. Tomasi, M. Cossi, N. Rega, J. M. Millam, M. Klene, J. E. Knox, J. B. Cross, V. Bakken, C. Adamo, J. Jaramillo, R. Gomperts, R. E. Stratmann, O. Yazyev, A. J. Austin, R. Cammi, C. Pomelli, J. W. Ochterski, R. L. Martin, K. Morokuma, V. G. Zakrzewski, G. A. Voth, P. Salvador, J. J. Dannenberg, S, Dapprich, A. D. Daniels, Ö. Farkas, J. B. Foresman, J. V. Ortiz, J. Cioslowski, D. J. Fox, Gaussian 09, Revision D.01, Gaussian, Inc., Wallingford, CT, 2009.

34. T. A. Keith, AIMALL, version 13.05.06; TK Gristmill Software, Overland Park KS, 2013; aim.tkgristmill.com.

35. I. Mata, I. Alkorta, E. Espinosa, E. Molins, *Chem. Phys. Lett*. 2011, **507**, 185-189.

36. (a) R. Dovesi, R. Orlando, B. Civalleri, R. Roetti, V. R. Saunders, C. M. Zicovich-Wilson, *Z. Kristallogr*. 2005, **220**, 571; (b) R. Dovesi, V. R. Saunders, R. Roetti, R. Orlando, C. M. Zicovich-Wilson, F. Pascale, B. Civalleri, K. Doll, N. M. Harrison, I. J. Bush, P. D'Arco, M. Llunell, *CRYSTAL09*, 2009, CRYSTAL09 User's Manual, University of Torino, Torino.

37. **(**a) A. D. Becke, *J. Chem. Phys.* 1993, **98**, 5648; (b) C. Lee, W. Yang, R. G. Parr, *Phys. Rev. B* 1988, **37**, 785.

38. (a) L. L. Presti, R. Destro, *J. Chem. Phys.* 2008, **128**, 044710; (b) de Vries, R. Y.; Feil, D.; Tsirelson, V. G. *Acta Crystallogr., Sect. B* 2000, **56**, 118; (c) Bytheway, I.; Chandler, G. S.; Figgis, B. N. *Acta Crystallogr., Sect. A* 2002, **58**, 451; (d) Volkov, A.; Abramov, Y.; Coppens, P.; Gatti, C. *.Acta Crystallogr., Sect. A* 2000, **56**, 332; (e) Coppens, P.; Volkov, A. *Acta Crystallogr.Sect. A* 2004, **60**, 357.

39. A. Volkov, P. Macchi, L. J. Farrugia, C. Gatti, P. Mallinson, T. Richter, T. Koritsanszky, *XD2006, Rev. 5.34*; University at Buffalo, State University of New York: Buffalo, NY, USA, 2006.

40. N. K. Hansen, P. Coppens, *Acta Crystallogr. Sect. A* 1978, **34**, 909–921.

41. (a) Z. Su, P. Coppens, *Acta Crystallogr. Sect. A* 1998, **54**, 646−652. (b) P. Macchi, P. Coppens, *Acta Crystallogr. Sect. A* 2001, **57**, 656–662.

42. F. H. Allen, *Acta Crystallogr.* 1986, **B42**, 515–522.

43. L. H. R. Dos Santos, A. Krawczuk, P. Macchi, *J. Phys. Chem. A*. 2015, **119**, 3285−3298.

44. M; Stojanovic, M. Baranac-Stojanovic, *J. Org. Chem.* 2016, **81**, 197–205.

45. Y. -F. Yanq, Y. Lianq, F. Liu, K. N. Houk, *J. Am. Chem. Soc.* 2016, **138**, 1660-1667.

46. C. B. Hubschle, B. Dittrich, *J. Appl. Cryst.* 2011. **44**, 238-240.